Plasma Chemistry and Plasma Processing
https://doi.org/10.1007/s11090-024-10516-1

ORIGINAL PAPER

Towards the Understanding of Parameters Allowing to Anticipate the Precipitation Reaction of Metallic Precursors in Humid Air Gliding Arc Plasma Reactor

F. Hanon[1] · M. Devillers[1] · E. M. Gaigneaux[1]

Received: 22 July 2024 / Accepted: 20 September 2024

Abstract
The humid air gliding arc plasma (GP) has demonstrated its capability to synthesize catalysts (metal (hydr)oxides and supported catalysts) with intriguing properties and significant catalytic activity while employing interesting synthesis conditions compared to conventional catalyst synthesis. However, previous studies exposed various precursors to the plasma without prior knowledge of their reactivity through GP. The objective of this paper is to investigate the parameters influencing precursor reactivity and precipitation under humid air GP, by identifying commonalities between reactive and non-reactive precursors. Several factors were identified as predominant: the solubility of the precursor and precipitate, the acidification of the medium along exposure, the redox potential of reactions between the precursor and HNO_2/NO_2^- species plasma-generated, and the metal precursor nature. These identified factors have enabled us to create a dichotomous key that can be used for any type of precursors, allowing to anticipate their potential precipitation when exposed to the GP. By utilizing this key, we have identified two new precursors that react, forming new types of solids never synthesized before by GP: Au and Ru-based solids. This demonstrates that GP may be a promising method for developing new types of catalysts, such as metal-supported catalysts, but also indicates that a limited number of precursors may react, at least without changing the conventional synthesis parameters. Therefore, this article highlights both the possibilities and limitations of GP catalyst synthesis.

Keywords Glidarc plasma · Catalysts · Precipitation · Metal precursors · Solubility · pH · Redox

Introduction

Due to their significant contributions to both the economic viability and environmental sustainability of chemical industries, catalysts are utilized in over 90% of all industrial chemical transformations across various sectors, including polymers, pharmaceuticals,

✉ E. M. Gaigneaux
eric.gaigneaux@uclouvain.be

[1] Institute of Condensed Matter and Nanosciences (IMCN), Université Catholique de Louvain (UCLouvain), Place Louis Pasteur 1, 1348 Louvain-La-Neuve, Belgium

agrochemicals, and petrochemicals [1]. As a result, ongoing research in catalysts synthesis aims to enhance their properties and performances in a wide variety of reactions [2]. Numerous liquid-phase techniques have been developed to create these catalysts, such as sol–gel and precipitation processes, the last one being widely used industrially. However, despite their advantages, such as their well-established nature and ability to generate catalysts with a wide range of interesting properties (including porosity, specific surface area, stability, purity, etc.), they also possess inherent drawbacks. Among the primary disadvantages are the high cost of the precursor materials, the time-consuming nature of the synthesis, the meticulous parameters control during the whole synthesis, the necessity of adding numerous substances that induce precipitation, and the utilization of environmentally harmful solvents. Consequently, the pursuit of new synthesis methodologies capable of mitigating these shortcomings while still yielding catalysts with desirable properties remains an exciting field of research. It is within this context that the utilization of plasma, as a novel synthesis method for catalysts, emerges as a promising objective [3]. Among the various types of plasma used for catalysts preparations, gliding arc plasma stands out due to its "non-thermal" properties. It combines the benefits of both thermal, through the reactive species it generates, and non-thermal plasma, by operating at atmospheric pressure and low temperatures [3, 4].

The glidarc plasma reactor was invented by H. Lesueur and further developed by A. Czernichowski in 1988 [5, 6]. It consists of two stainless steel electrodes with a divergent profile that are connected to a high-voltage generator. When the generator is activated, an arc forms at the smallest distance between the electrodes. Then, a flow of gas (plasma gas) is directed perpendicular to the arc, pushing it along the electrodes. At the end of these electrodes, as the distance between them increases, the arc cannot be sustained, and a new discharge can begin at the smallest distance between the electrodes. In this system, the arc (which constitutes the thermal part of the plasma) is cooled down to approximately ambient temperature by the gliding process and bursts into a plume of quenched plasma at atmospheric pressure (Fig. 1) [5, 7–12]

The plasma plume comprises a variety of species, including electrons, cations and free radicals, all of which possess reactivity that can be used to carry out chemical reactions in and/or on gas, solid or liquid targets. When humid air is employed as plasma gas, the species produced are known to have mostly acidic and oxidant effects on the target. Plasma gas interacts with the arc's electrons (and photons), forming activated species, ions, and radicals, known as "primary species". In addition to these radicals, "secondary species" can be formed when primary species react with each other or with parent species (Fig. 1). Among all these species generated in humid air plasma, some are considered as "short-lived species" such as the radicals OH°, NO°, O°; etc. (with lifetime in the nanosecond range), while some are "long-lived species" such as H_2O_2, HNO_3, HNO_2, etc. (lifetime > 1 s) (Fig. 1). Only species with longer lifespans have the capability to transit through and react within the bulk liquid, whereas shorter-lived species only induce reactions at the gas–liquid interface [8, 10, 12–23].

The humid air glidarc plasma reactor's acidifying, oxidizing, and reducing features make it highly interesting for a wide variety of applications, including water and air depollution, hydrogen production, hydrocarbon oxidation and conversion, and modification of solid surface properties [5, 10, 12, 25]. Furthermore, this method has already demonstrated its ability to synthesize catalysts such as metal (hydr)oxides (TiO_2, FeO_x, MnO_2, SnO_2, WO_3) and supported catalysts (FeO_x/Kaolinite, TiO_2/SnO_2) with good properties and interesting catalytic activity when used for pollutant degradation in both gaseous and liquid phases (Table 1) [13, 14, 22, 26–29]. In addition to the interesting catalysts developed,

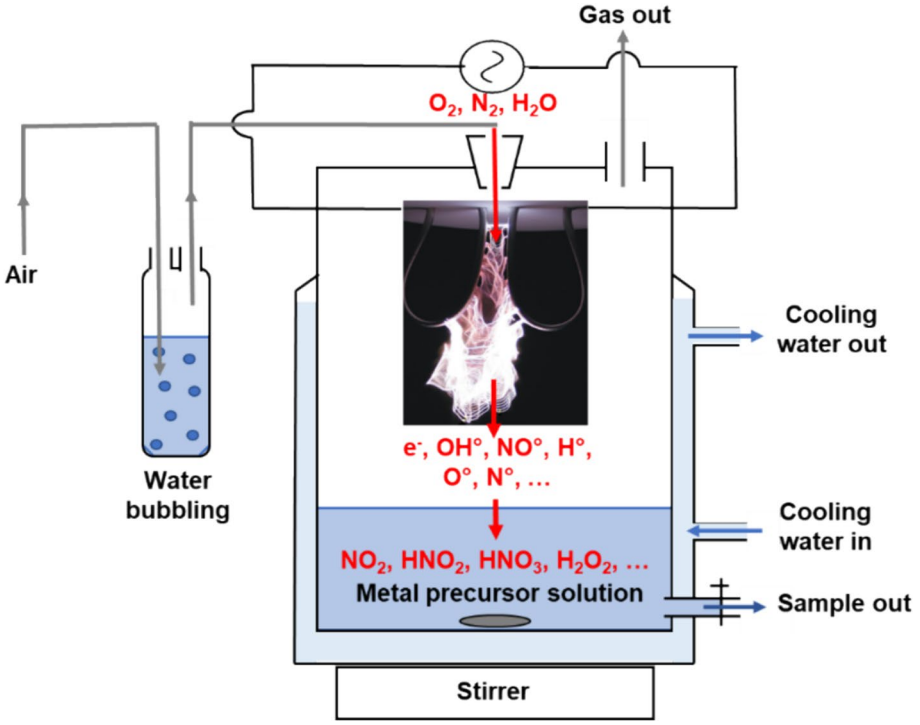

Fig. 1 Scheme and species created in humid air glidarc plasma reactor; plasma plume from [24]

Table 1 Catalysts synthesized by humid air glidarc plasma in the literature [14, 28, 30–32]

Precursor	Catalyst synthesized	Synthesis reaction
$TiCl_3$	TiO_2 [14, 33]	$TiCl_3 + OH° + H_2O \rightleftharpoons TiO_2 + 3HCl$
$TiCl_3 + SnCl_2.2H_2O$	TiO_2/SnO_2 [26]	$TiCl_3 + SnCl_2 + 3OH° + H_2O \rightleftharpoons TiO_2/SnO_2 + 5HCl$
$(NH_4)_2Fe(SO_4)_2.6H_2O$	FeOOH [13, 31]	$Fe^{2+} + OH° \rightleftharpoons Fe^{3+} + OH^-$ $Fe^{3+} + 2OH^- + H_2O \rightleftharpoons FeOOH + H_3O^+$
	Fe_2O_3 [31, 34]	$2FeOOH \overset{calcination}{\rightarrow} Fe_2O_3 + H_2O$
Mayouom Kaolinite + $(NH_4)_2Fe(SO_4)_2.6H_2O$	FeO_x/kaolinite[31]	$Fe^{2+} + OH° \rightleftharpoons Fe^{3+} + OH^-$ $Fe^{3+} + 2OH^- + H_2O \rightleftharpoons FeOOH + H_3O^+$
$KMnO_4$	α-MnO_2 and γ-MnO_2 [22, 29, 30]	$MnO_4^- + NO° \rightleftharpoons MnO_2 + NO_3^-$
$Mn(CH_3COO)_3.2H_2O$	γ-MnO_2 and β-MnO_2 [22]	$Mn^{3+} + OH° + H_2O \rightleftharpoons MnO_2 + H^+$
$SnCl_2.2H_2O$	SnO_2 [28]	$SnCl_2 + H_2O \rightleftharpoons Sn(OH)Cl + HCl$ $Sn(OH)Cl + 3OH° \rightleftharpoons SnO_2 + 2H_2O + \frac{1}{2}Cl_2$
$Na_2WO_4.2H_2O$	WO_3 [32]	$Na_2WO_4.2H_2O + 2NO° \rightleftharpoons WO_3.2H_2O + 2\left(Na^+ + NO_3^-\right)$

glidarc plasma synthesis also provides interesting synthesis conditions in comparison to conventional catalysts synthesis processes. The most significant advantage of this method is that it operates under mild conditions and has a short processing time. Furthermore, this approach may be considered eco-friendly and cost-effective because the sole chemical utilized to form reactive species is water-saturated air, which is non-polluting, available and renewable [13].

However, despite the utilization of various types of precursors in previous literature, which have demonstrated the efficacy in precipitating oxides or hydroxides, we still lack understanding regarding why these precursors work. It remains uncertain whether every type of metal precursor is capable of reacting and forming a precipitate via glidarc plasma. Until now, we have simply exposed precursors to the plasma without prior knowledge of whether they were the right choice. Consequently, we are unable to explain why certain precursors react while others do not. This lack of understanding makes it challenging to ascertain the potential versatility of the method in synthesizing various types of catalysts.

Therefore, the objective of this paper is to investigate the parameters influencing the ability of certain precursors to react via humid air glidarc plasma, forming a precipitate. The aim is to enhance our understanding of the method, ultimately enabling the synthesis of a broader range of catalysts. This, in turn, could enhance the interest of GP as an innovative method for catalysts synthesis.

To fulfil this objective, the strategy was to identify commonalities between precursors that do form a precipitate via glidarc plasma and those that do not react. To achieve this, several precursors were tested to establish a pool of both reactive and non-reactive precursors.

To determine the factors dictating the ability of the precursors to react, the strategy was to draw inspiration from the factors that affect the classical synthesis of catalysts by precipitation, which shares many similarities with synthesis via GP exposure. Furthermore, it involved revisiting the basics of chemistry and conducting calculations to theoretically rationalized the plasma reactions. Additionally, insights from previous research were valuable as it was found that among the plasma species created, the long-lived species, especially HNO_2/NO_2^-, predominantly impact the oxidoreduction of the precursors [35].

Several factors were identified as predominant, including medium pH, redox potential of reactions between the precursor and HNO_2/NO_2^- species plasma-generated, precipitate solubility and of course the nature of the metal precursor.

Materials and Methods

Materials

$Al(NO_3)_3.9H_2O$ (≥ 95%), $AlCl_3$ (99%), $HAuCl_4.3H_2O$ (99%), $K_2Cr_2O_7$ (≥ 99%), $Fe(NO_3)_3.9H_2O$ (≥ 98%), $FeCl_3.6H_2O$ (≥ 99%), $FeSO_4.7H_2O$ (≥ 99%), $Mn(CH_3COO)_3.2H_2O$ (97%), $Mn(CH_3COO)_2.3H_2O$ (99.99%), $NaMnO_4$ (solution 40% wt in H_2O), $MnSO_4.H_2O$ (≥ 99%), $Na_2MoO_4.2H_2O$ (≥ 99%), $Ni(NO_3)_2.6H_2O$ (≥ 97%), $Ni(CH_3COO)_2.4H_2O$ (98%), $SnSO_4$ (≥ 95%), $SnCl_2$ (≥ 99%), $TiCl_3$ (solution 10–15% in HCl) were purchased from Sigma Aldrich.

$Bi(NO_3)_3.5H_2O$ (≥ 98%), $Co(NO_3)_2.6H_2O$ (≥ 98%), $(NH_4)_2Fe(SO_4)_2.6H_2O$ (≥ 99%), $KMnO_4$ (≥ 99%), $Mn(NO_3)_2.4H_2O$ (≥ 98%), $MnCl_2$ (97%), $Na_2WO_4.2H_2O$ (≥ 99%) were obtained from Roth.

$AgNO_3$ (99.9%), $AgCH_3COO$ (99%), $Fe(CH_3COO)_2$ (95%), $MnCl_2$ (97%), $(NH_4)_2PtCl_4$ (99.99%), $Ti(SO_4)_2$ (15% (w/v) solution in diluted sulfuric acid), $KRuO_4$ (97%) were obtained from Thermo Scientific.

All the solutions were prepared with demineralized water as solvent.

Methods

Synthesis Device: The GP Reactor

The gliding arc plasma system employed in this study comprises the following components (**Error! Reference source not found.**):

- A high voltage generator (ABL Transformer; 9 kV; 100 mA) connected to both stainless-steel electrodes with a divergent profile, positioned within the reactor.
- A gas supply setup consisting of a compressed air source, a saturator filled with water in which air is bubbled, and a flowmeter controlling the gas flow rate (fixed at ≈ 400 L/h).
- A central reactor in the form of a double-walled cylindrical glass tube. It features inlets and outlets for the circulation of an external cooling fluid (water), an additional inlet for the nozzle to direct the air flow between the electrodes, and an opening for the gas exhaust (to prevent exceeding pressure within the reactor). An outlet valve is also present to facilitate retrieval of the reactor content following plasma exposure.

Precursors Exposure and Solid Recovery

Various metal precursors were exposed to the glidarc plasma to establish a pool of both reactive and non-reactive precursors (Table 2).

The precursor solutions were prepared by dissolving these compounds in deionized water to obtain a certain concentration (Table 2). Subsequently, 450 mL of the respective solutions were introduced into the reactor, stirred magnetically (1 rotation/s), and exposed

Table 2 Type and concentrations of precursors exposed to the glidarc plasma

Concentration (mol/L)	Metal	Precursor
0.001	Au, Ru, Bi, Pt	$HAuCl_4.3H_2O$, $KRuO_4$, $Bi(NO_3)_3.5H_2O$, $(NH_4)_2PtCl_4$
0.01	Ag, Cr, Co, Fe, Mn, Mo, Ni, Sn, Ti, W	$AgNO_3$, $AgCH_3COO$, $K_2Cr_2O_7$, $Co(NO_3)_2.6H_2O$, $Fe(NO_3)_3.9H_2O$, $FeCl_3.6H_2O$, $FeSO_4.7H_2O$, $Fe(CH_3COO)_2$, $(NH_4)_2Fe(SO_4)_2.6H_2O$, $Mn(NO_3)_2.4H_2O$, $MnCl_2$, $MnSO_4.H_2O$, $Mn(CH_3COO)_3.2H_2O$, $Mn(CH_3COO)_2.3H_2O$, $KMnO_4$, $NaMnO_4$, $Ni(NO_3)_2.6H_2O$, $Ni(CH_3COO)_2.4H_2O$, $SnCl_2$, $SnSO_4$, $Ti(SO_4)_2$, $Na_2WO_4.\ 2H_2O$
0.02	Al	$Al(NO_3)_3.9H_2O$, $AlCl_3$
0.03	Mo	$Na_2MoO_4.2H_2O$
2	Ti	$TiCl_3$

to the plasma discharge for maximum 2 h. If no solid formed within this time frame, we assumed that the precursors did not react to form a precipitate via glidarc plasma.

The pH of the precursor solution was measured using a pH meter before and after exposure to the plasma.

If a solid precipitate was obtained after exposure to the plasma discharge, it was recovered by centrifugation (24490 G, 30 min) and subjected to two washing cycles with distilled water. The solids obtained after centrifugation were subsequently dried in an oven under air at 110 °C for 22 h ± 2 h.

Characterization of the Solids Formed: X-Ray Diffraction (XRD)

XRD analyses are performed when precursors reacted by GP have formed a precipitate. The solid, previously ground, is placed on a polished Si single crystal sample holder covered with a thin layer of Nivea© cream and is introduced into a Bruker-D8 Advance diffractometer with a Bragg–Brentano geometry. The X-rays sent to the sample are produced using a copper anode ($K_\alpha = 0.15418$ nm) operated 1200 watts, 30 mA and 40 kV. The analysis is performed for angles $2\theta = 5°$ to 80° with an increment of 0.015° and 0.15 s integration time. Detection is performed using a LynxEye XE-T Technology detector. The diffractograms are then processed using the ICDD-PDF2-2004 database [36].

Results and Discussion

Factors Influencing the Ability of a Precursor to React

As previously explained, the GP catalysts synthesis shares many similarities with the classical synthesis involving a precipitation process. Therefore, it was anticipated that similar factors influencing the precipitation method would also be important in our case. Among these factors, the pH of the medium, the nature of the precursor used, and the solubility of the precipitate will be discussed. However, one specific factor arises from the plasma species, namely HNO_2 and NO_2^-, generated from the humid air GP and which trigger the redox reaction of precursor exposed to the medium. This factor is the potential of the redox couple involved in the reaction.

pH of the Medium

As suggested in previous literature, acidic species such as HNO_3 and HNO_2 are among those created by the plasma [12, 17, 35]. These species decrease the pH of the solution during the exposure, reaching a pH around 3, if only distilled water is exposed. The pH stabilizes around this value due to the buffering effect of the HNO_2/NO_2^- couple (pKa = 3.3) [37]. In fact, as shown in Table 3, the final pH of the exposed precursor solution often stabilizes around this value, except when the metal precursor can act as a secondary buffer, as observed with acetate precursors. However, not all types of solids form under such acidic conditions. Therefore, we suggest that the first factor influencing the ability of a precipitate to form under glidarc plasma is this acidification of the medium during the exposure.

To investigate this hypothesis, the Pourbaix diagrams of the various metals tested by glidarc plasma are of primary interest (Fig. 2 as example, Supplementary information SI.2 for other metals) [38]. In these diagrams, the x-axis represents the pH of the medium, while

Table 3 Precursors exposed to the glidarc plasma, solution's pH before and after exposure, and type of solid that can be formed in water with the pH range they can exist in

Metal	Precursor	Initial pH	Precipitate ?	Final pH	Precipitate that can be formed in water [38]	
					Type	pH range
Ag	$AgNO_3$	5	No	3	Ag; Ag_2O	[0–14]; [8–14]
	$AgCH_3COO$	6.4	No	5.2		
Al	$Al(NO_3)_3.9H_2O$	3.5	No	2	Al_2O_3	[2.5–12.5]
	$AlCl_3$	3.6	No	3.2		
Bi	$Bi(NO_3)_3.5H_2O$	2	No	2.4	Bi_2O_3; Bi	[4.5–14]; [0–14]
Co	$Co(NO_3)_2.6H_2O$	2.5	No	2	$Co(OH)_3$; $Co(OH)_2$; Co	[5–14]; [7-14]; [5–14]
Cr	$K_2Cr_2O_7$	4.3	No	2.9	Cr_2O_3	[3.5–14]
Fe	$Fe(NO_3)_3.9H_2O$	2.5	No	2.3	$Fe(OH)_3$; $Fe(OH)_2$	[0.5–14]; [6–14]
	$FeCl_3.6H_2O$	2.5	No	2.4		
	$Fe(CH_3COO)_2$	5.4	No	5.2		
	$FeSO_4.7H_2O$	4.1	Yes (FeOOH)* [39, 40]	3		
	$(NH_4)_2Fe(SO_4)_2.6H_2O$	3	Yes (FeOOH)* [13, 39, 40]	3		
Mn	$Mn(NO_3)_2.4H_2O$	4.1	No	3.1	MnO_2; Mn_2O_3; Mn_3O_4; $Mn(OH)_2$	[0–14]; [4.5–14]; [7–14]; [8.5–14]
	$MnCl_2$	4.9	No	3.2		
	$MnSO_4.H_2O$	5.4	No	3.3		
	$Mn(CH_3COO)_3.2H_2O$	5	Yes ($MnO(OH)$, MnO_2)* [22]	4.8		
	$Mn(CH_3COO)_2.3H_2O$	6.1	No	5.4		
	$KMnO_4$	6.9	Yes: ($KMnO_2$) ** [22, 29, 41]	3.2		
	$NaMnO_4$	6.8	Yes: (MnO_2)*	3.2		
Mo	Na_2MoO_4	6.7	No	5.4	MoO_3; MoO_2	[0–1.5]; [3–8.5]
Ni	$Ni(NO_3)_2.6H_2O$	5.2	No	3.2	Ni_3O_4; $Ni(OH)_2$; Ni	[4.5–14]; [7–14]; [5.5–14]
	$Ni(CH_3COO)_2.4H_2O$	6	No	5.7		
Pt	$(NH_4)_2PtCl_4$	6.2	No	2.7	PtO_2; $Pt(OH)_2$; Pt	[0–14]
Sn	$SnCl_2$	2.5	Yes (SnO_2)* [28, 39, 40]	1.9	SnO_2	[0–14]
	$SnSO_4$	2.6	Yes (SnO_2)* [39, 40]	2.1		

Table 3 (continued)

Metal	Precursor	Initial pH	Precipitate ?	Final pH	Precipitate that can be formed in water [38]	
					Type	pH range
Ti	$Ti(SO_4)_2$	1.7	No	1.6	TiO_2	[0–14]
	$TiCl_3$		Yes (TiO_2) [33]	1.8		
W	$Na_2WO_4.2H_2O$	6.7	No	6.2	WO_3	[0–6]

*Pictures and diffractograms of the formed solids, which enable us to identify the developed phases, are presented in supplementary information SI.1. It is important to note that varying synthesis conditions, such as incorporating a calcination step, a post-discharge step, or using a "no-cooling system", can lead to different characteristics in the synthesized solids, including variations in phase type, morphology, and textural properties. These findings are discussed in detail in other published articles [13, 22, 28, 29, 33, 39–41]

**The $KMnO_2$ phase is actually a polymorph of MnO_2 (birnessite) that is non-stoichiometrically composed. In this structure, K^+ ions are inserted into the channel of the materials, and some Mn^{4+} ions are either missing, or replaced by Mn^{3+} ions [30]

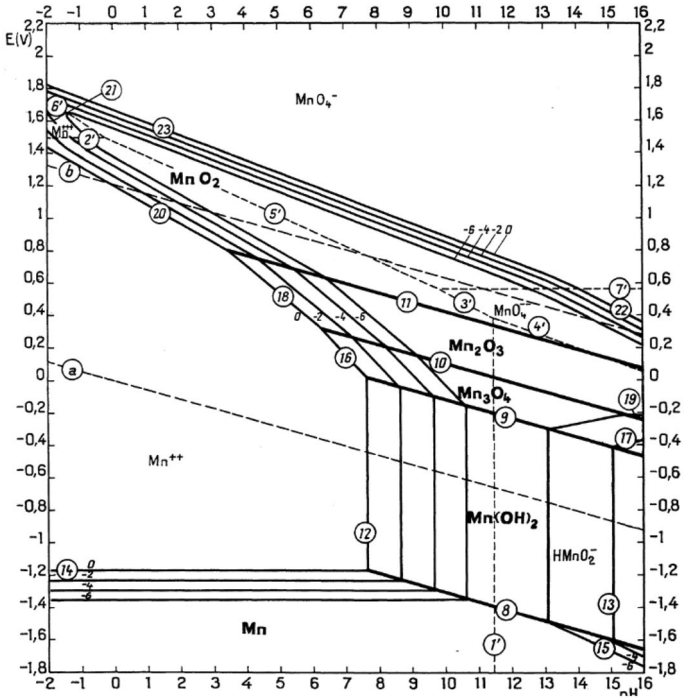

Fig. 2 Pourbaix diagram of Mn-water at 25 °C (considering β-MnO_2 (pyrolusite)) [38]

the y-axis represents the voltage potential with respect to the standard hydrogen electrode. Furthermore, it should be noted that the dashed "a" and "b" lines in this diagram refer to the thermodynamic limitations corresponding to the redox behaviour of water itself, which is here the solvent. From a thermodynamic point of view, only species comprised between these lines should therefore exist in water. However, kinetic limitations could allow for the stabilization of metastable species under certain conditions [38].

To simplify the interpretation of these diagrams and understand the types of precipitates that can potentially form, we have compiled in Table 3 the solids that can form in water for all the metal tested, along with the approximate pH range where they can be created. To determine this range, we used the "-2" line on the Pourbaix diagram as a limit, as it represents the equilibrium between solid and soluble substances when the concentration of the dissolved substance is 10^{-2} mol/L, corresponding to the quantity of metal ions in our solution due to the initial concentration of precursors we chose [38]. By comparing this range to the final pH of the exposed solution, we observe that some precipitates cannot form at such pH which explains why they are not formed (marked in black). Furthermore, it is worth noting that all the precursors reacting via glidarc plasma have a final pH within the range of the corresponding solid formed (marked in green). This indicates that the pH of the medium is an important factor in determining whether a precursor can react via glidarc plasma to form a precipitate.

However, we also observed that some precursors can normally form certain solids at the final pH of the solution after exposure but still do not produce any precipitate (marked in red). This suggests that other factors need to be considered.

Potential of the Redox Reaction

The second important factor can be illustrated using the Mn precursors as an example. While Mn(III) and Mn(VII) precursors react by plasma to form MnO_2, Mn(II) does not. This underlines the significance of another important factor: the oxidation state, or more precisely, the standard potential of the redox couple in which the metallic ion is involved (M^{n+}/precipitate).

As mentioned in the introduction, we previously discovered that the long-lived species, especially HNO_2 and/or NO_2^-, are the main species initiating the precipitation process of precursors exposed to the glidarc plasma [35]. These species have the ability to undergo redox reactions with the precursor, that could induce precipitation. Actually, HNO_2 and NO_2^- exhibit dual properties and can function either as oxidants or reducers in diverse types of redox couples [38]. In this first approach, as redox reactions are known to be kinetically favoured when less electrons are involved, we focused on reactions involving a single electron transfer for the redox couple where HNO_2 or NO_2^- species are involved (Table 4) [42]. Knowing this, it is possible to evaluate their ability to undergo a redox reaction by calculating the difference in standard potential ($\Delta E°$) and equilibrium constant (K) of the 2 couples reacting together (Eq. 1). In a previous article, we already performed this analysis for all the precursors known to undergo a redox reaction by glidarc plasma (Fe^{2+}, MnO_4^-, Sn^{2+} and Ti^{3+}), demonstrating that the redox reaction followed by the precipitation process of precursors triggered by the HNO_2 or NO_2^- species is indeed theoretically feasible, as $\Delta E° > 0$ and $K > 10^3$ (Eq. 1) [35].

$$K = \exp\left(\frac{nF\Delta E°}{RT}\right) \tag{1}$$

where F = 96485C; R = 8.314 J/mol; T = 298 K;$\Delta E° = E°_{ox} - E°_{red}$

However, previous calculations were made considering the E°, the standard equilibrium potential of the reaction at 25 °C. This value does not account for the actual concentration of ionic species or the pH of the medium. The real E in our medium for a couple $\varepsilon aA + mH^+ + ne^- \rightleftharpoons bB + cH_2O\varepsilon$ can be calculated using the Eq. 2 [36, 38]:

$$E = E° + \frac{0.059}{n}\log\left(\frac{(C_A)^a}{(C_B)^b}\right) - 0.059\left(\frac{m}{n}\right)pH \tag{2}$$

Given that we know the pH of the medium after exposure of each precursor and the concentration used for each, it is possible to calculate the actual E for all the redox couples considered. However, since the exact concentrations of HNO_2 and NO_2^- in our medium are unknown, it is not possible to calculate the actual E for their redox couple. Therefore, we

Table 4 Redox couples where HNO_2 or NO_2^- act as oxidants and reducers with only 1 electron involved [38]

	When HNO_2 or NO_2^- act as oxidant	When HNO_2 or NO_2^- act as reducer	E° (V/NHE)	Equation number
Oxidant	$NO_2^- + 2H^+ + e^-$	$NO°_{(g)} + H_2O$	1.2	Eq. 3
	$HNO_2 + H^+ + e^-$	$NO° + H_2O$	1.00	Eq. 4
Reducer	$NO_2 + e^-$	NO_2^-	0.9	Eq. 5
	$NO_2 + H^+ + e^-$	HNO_2	1.09	Eq. 6

Table 5 Redox reactions between HNO_2 or NO_2^- species and precursors exposed to the glidarc plasma that give a precipitate [35]

Reduction of the precursors		
$KMnO_4$; $NaMnO_4$ [38]:		
$MnO_4^- + 4H^+ + 3e^- \rightleftharpoons MnO_2 + 2H_2O$		
$E = 1.692 - 0.0788pH + 0.0197log\left(C_{MnO_4^-}\right) = 1.41V$		
NO_2/NO_2^- (Eq. 5) $E° = 0.9$ V	$MnO_4^- + 4H^+ + 3NO_2^- \rightleftharpoons MnO_2 + 2H_2O + 3NO_2$	$\Delta E = 0.51$ V
NO_2/HNO_2 (Eq. 6) $E° = 1.09$ V	$MnO_4^- + H^+ + 3HNO_2 \rightleftharpoons MnO_2 + 2H_2O + 3NO_2$	$\Delta E = 0.32$ V
Oxidation of the precursor		
$FeSO_4.7H_2O$; $(NH_4)_2Fe(SO_4)_2.6H_2O$ [38]:		
$FeOOH + 3H^+ + e^- \rightleftharpoons Fe^{2+} + 2H_2O$		
$E = 0.77 - 0.1773pH - 0.0591log\left(C_{Fe^{2+}}\right) = 0.36V$		
$NO_2^-/NO°$ (*Eq.*3) $E° = 1.2$ V	$Fe^{2+} + H_2O + NO_2^- \rightleftharpoons FeOOH + H^+ + NO$	$\Delta E = 0.84$ V
$HNO_2/NO°$ (*Eq.*4) $E° = 1.00$ V	$Fe^{2+} + H_2O + HNO_2 \rightleftharpoons FeOOH + 2H^+ + NO$	$\Delta E = 0.64$ V
$SnSO_4$; $SnCl_2$ [38]:		
$SnO_2 + 4H^+ + 2e^- \rightleftharpoons Sn^{2+} + 2H_2O$		
$E = -0.077 - 0.1182pH - 0.0295log\left(C_{Sn^{2+}}\right) = -0.26V$		
$NO_2^-/NO°$ (*Eq.*3) $E° = 1.2$ V	$Sn^{2+} + 2NO_2^- \rightleftharpoons SnO_2 + 2NO°$	$\Delta E = 1.46$ V
$HNO_2/NO°$ (*Eq.*4) $E° = 1.00$ V	$Sn^{2+} + 2HNO_2 \rightleftharpoons SnO_2 + 2NO° + 2H^+$	$\Delta E = 1.26$ V
$TiCl_3$ [38]:		
$TiO_2 + 4H^+ + e^- \rightleftharpoons Ti^{3+} + 2H_2O$		
$E = -0.666 - 0.2364pH - 0.0591log\left(C_{Ti^{3+}}\right) = -1.11V$		
$NO_2^-/NO°$ (*Eq.*3) $E° = 1.2$ V	$Ti^{3+} + H_2O + NO_2^- \rightleftharpoons TiO_2 + 2H^+ + NO$	$\Delta E = 2.31$ V
$HNO_2/NO°$ (*Eq.*4) $E° = 1.00$ V	$Ti^{3+} + H_2O + HNO_2 \rightleftharpoons TiO_2 + 3H^+ + NO$	$\Delta E = 2.11$ V

Table 6 Redox reactions between HNO_2 or NO_2^- species and precursors exposed to the glidarc plasma that do not give a precipitate

Reduction of the precursors		
$AgNO_3$; $AgCH_3COO$ [38]:		
$Ag^+ + e^- \rightleftharpoons Ag$		
$E_0 = 0.799 + 0.0591 log\left(C_{(Ag^+)}\right) = 0.68V$		
NO_2/NO_2^- (Eq. 5)	$Ag^+ + NO_2^- \rightleftharpoons Ag + NO_2$	$\Delta E = -0.22$ V
$E° = 0.9$ V		
NO_2/HNO_2 (Eq. 6)	$Ag^+ + HNO_2 \rightleftharpoons Ag + NO_2 + H^+$	$\Delta E = -0.41$ V
$E° = 1.09$ V		
$Bi(NO_3)_3$ [38]:		
$Bi^{3+} + 3e^- \rightleftharpoons Bi$		
$E_0 = 0.215 + 0.0197 log\left(C_{Bi^{3+}}\right) = 0.16V$		
NO_2/NO_2^- (Eq. 5)	$Bi^{3+} + 3NO_2^- \rightleftharpoons Bi + 3NO_2$	$\Delta E = -0.74$ V
$E° = 0.9$ V		
NO_2/HNO_2 (Eq. 6)	$Bi^{3+} + 3HNO_2 \rightleftharpoons Bi + 3NO_2 + 3H^+$	$\Delta E = -0.93$ V
$E° = 1.09$ V		
Na_2MoO_4 [38]:		
$MoO_4^{2-} + 4H^+ + 2e^- \rightleftharpoons MoO_2 + 2H_2O$		
$E_0 = 0.606 - 0.1182pH + 0.0295 log\left(C_{MoO_4^{2-}}\right) = -0.09V$		
NO_2/NO_2^- (Eq. 5)	$MoO_4^{2-} + 4H^+ + 2NO_2^- \rightleftharpoons MoO_2 + 2H_2O + 2NO_2$	$\Delta E = -0.99V$
$E° = 0.9$ V		
NO_2/HNO_2 (Eq. 6)	$MoO_4^{2-} + 2H^+ + 2HNO_2 \rightleftharpoons MoO_2 + 2H_2O + 2NO_2$	$\Delta E = -1.18V$
$E° = 1.09$ V		
$Ni(CH_3COO)_2$ [38]:		
$Ni^{2+} + 2e^- \rightarrow Ni$		
$E_0 = -0.250 + 0.0295 log\left(C_{Ni^{2+}}\right) = -0.31V$		

Table 6 (continued)

NO_2/NO_2^- (Eq. 5) $E° = 0.9$ V	$Ni^{2+} + 2NO_2^- \rightarrow Ni + 2NO_2$	$\Delta E = -1.21$ V
NO_2/HNO_2 (Eq. 6) $E° = 1.09$ V	$Ni^{2+} + 2HNO_2 \rightarrow Ni + 2NO_2 + 2H^+$	$\Delta E = -1.4$ V
Oxidation of the precursor		
$\underline{Ni(CH_3COO)_2}$ [38]: $Ni_3O_4 + 8H^+ + 2e^- \rightleftharpoons 3Ni^{2+} + 4H_2O$ $E_0 = 1.977 - 0.2364pH - 0.0886log\left(C_{Ni^{2+}}\right) = 1.40V$		
$NO_2^-/NO°$ (*Eq*.3) $E° = 1.2$ V	$3Ni^{2+} + 2H_2O + 2NO_2^- \rightleftharpoons Ni_3O_4 + 4H^+ + 2NO$	$\Delta E = -0.2V$
$HNO_2/NO°$ (*Eq*.4) $E° = 1.00$ V	$3Ni^{2+} + 2H_2O + 2HNO_2 \rightleftharpoons Ni_3O_4 + 6H^+ + 2NO$	$\Delta E = -0.4V$

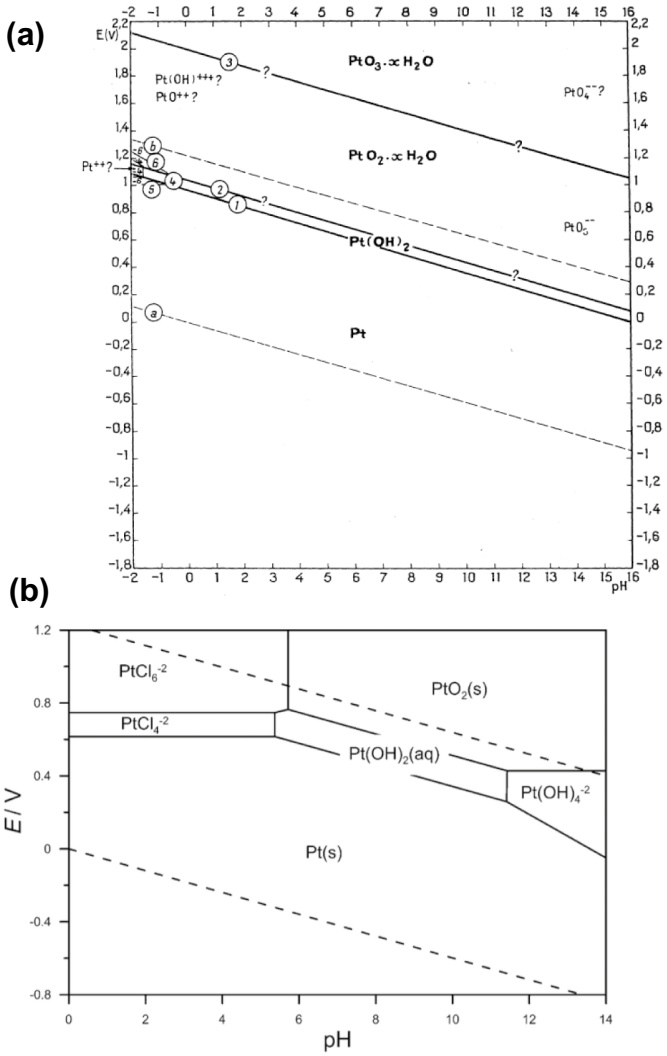

Fig. 3 Pourbaix diagram of **a** Pt-water at 25 °C [38]; **b** Pt-water containing 0.5 M of HCl at 25 °C [44]

will use the standard electrode potential (E°) for these species instead. Consequently, ΔE for each redox reaction was calculated using these accurate E values (Table 5, Table 6).

By considering the correct E value for the precursors reacting through GP (marked in green in the Table 3), calculated from the final pH obtained after exposure (Table 3) and the initial concentration of the precursor (Table 2), we still obtain $\Delta E > 0$ corresponding to a negative free enthalpy change G, indicating that they can indeed theoretically react with HNO_2 or NO_2^- species (Table 5).

Therefore, it may be possible to theoretically explain, with the same calculations, why all the other precursors, which are normally capable of forming a solid with a different oxidation state (OS) under the final pH obtained after exposure, do not seem to react by glidarc plasma (marked in red in the Table 3). By doing this, we observe that

Table 7 Redox reactions between HNO_2 or NO_2^- species and $(NH_4)_2PtCl_4$

$(NH_4)_2PtCl_4$ [43]: Where $K_f = 10^{16}$; $E°_{\frac{Pt^{2+}}{Pt}} = 1.2V$ $[PtCl_4]^{2-} + 2e^- \rightleftharpoons Pt + 4Cl^-$ $E° = 0.73 + 0.0295log\left(\frac{C_{[PtCl_4]^{2-}}}{(C_{[Cl^-]})^4}\right) = 0.924V$		
NO_2/NO_2^- (Eq. 5) $E° = 0.9$ V	$[PtCl_4]^{2-} + 2NO_2^- \rightleftharpoons Pt + 2NO_2 + 4Cl^-$	$\Delta E = 0.02$ V
NO_2/HNO_2 (Eq. 6) $E° = 1.09$ V	$[PtCl_4]^{2-} + 2HNO_2 \rightleftharpoons Pt + 2NO_2 + 2H^+ + 4Cl^-$	$\Delta E = -0.17$ V

in all cases, the redox reaction of these precursors with HNO_2 or NO_2^- species yields $\Delta E < 0$ (Table 6). Consequently, it is evident that these reactions cannot occur. This implies that the reason why these precursors do not yield to a solid after exposure to the GP is because they cannot undergo a redox reaction with the HNO_2 or NO_2^- species, which have been identified as the primary active species in the observed redox reactions [35].

Nature of the Precursor

Another aspect that we did not previously consider is that some precursors introduce other types of species that can impact the reactions occurring in the medium. In our earlier discussions, we only considered that the precursors dissolved to yield aqua ions when reacting with water molecules ($[M(OH_2)_N]^{z+}$, here noted as M^{z+}). However, some precursors are made of complex ions involving coordinating species like Cl^- and NH_3, and appear as such upon dissolution.

That is indeed what happens with $(NH_4)_2PtCl_4$. Upon dissolution, $[PtCl_4]^{2-}$ ions are present, as a result of the dissociation of the precursor [43]. To understand the influence of these complexes, we have to examine the Pourbaix diagram of Pt, both without and with the presence of Cl^- ions, as shown in Fig. 3 [44]. We observe that when Pt^{2+} is present as a complex $[PtCl_4]^{2-}$, its stability range is extended to a higher pH value (up to around 6). This diagram also shows that for Cl–Pt complexes, at the pH obtained after the exposure of the Pt precursor (2.7), PtO_2 can no longer be formed, and Pt is the only solid that can precipitate at this pH. This highlights the importance of considering the ions actually present in the solution after the dissolution of the precursor, and of taking into account, when necessary, the possible reactions these ions could undergo in solution.

Knowing this, it is possible to calculate ΔE for the redox reaction of $[PtCl_4]^{2-}$ with HNO_2 or NO_2^- to eventually form Pt (Table 7), calculated from the final pH obtained after GP exposure (Table 3) and the initial concentration of the precursor (Table 2). To do so, we need to consider the potential of the couple ML_y/M (Eq. 6) that can be calculated thanks to the formation constant (K_f) of the ML_y complex (Eq. 3) and the potential of the redox couple that does not imply the ligand, M^{n+}/M (Eq. 4).

For a neutral L ligand, the corresponding equations are:

$$M^{z+} + yL \rightleftharpoons \left[ML_y\right]^{z+} with K_f = \frac{\left[\left[ML_y\right]^{z+}\right]}{[M^{z+}][L]^y} \tag{3}$$

$$M^{z+} + ne^- \rightleftharpoons M with E_{\left(\frac{M^{z+}}{M}\right)} = E^\circ_{\left(\frac{M^{z+}}{M}\right)} - \frac{RT}{nF} \ln\left(\frac{1}{[M^{z+}]}\right) \tag{4}$$

$$\left[ML_y\right]^{z+} + ne^- \rightleftharpoons M + yL with E_{\left(\frac{\left[ML_y\right]^{z+}}{M}\right)} = E^\circ_{\left(\frac{\left[ML_y\right]^{z+}}{M}\right)} - \frac{RT}{nF} \ln\left(\frac{[L]^y}{\left[\left[ML_y\right]^{z+}\right]}\right) \tag{5}$$

$$E^\circ_{\left(\frac{\left[ML_y\right]^{z+}}{M}\right)} = E^\circ_{\left(\frac{M^{z+}}{M}\right)} - \left(\frac{RT}{nF}\right) \ln\left(K_f\right) \tag{6}$$

We can therefore see that considering the actual ions present in solution upon dissolution of the precursor is important to anticipate its potential reaction with plasma species and, consequently, its possible precipitation. In the case of the $(NH_4)_2PtCl_4$ precursor, precipitation is not possible because the ΔE for the redox reaction of $[PtCl_4]^{2-}$ with HNO_2 or NO_2^- is either very close to 0 or less than 0.

Solubility of the Precipitate

In addition to the precursors mentioned above, there are other precursors that did not precipitate and were not previously discussed. These include compounds that do not require a change of oxidation state (OS) to form the corresponding solid (Al^{3+}, Fe^{3+}, Ti^{4+}) (Table 3). For these precursors, a redox reaction is not the phenomenon required to initiate the precipitation. Instead, the formation of the precipitate depends solely on the concentration of ions present in the solution that participate in the formation of the solid. It is governed by the solubility of the precipitate that can be formed.

In fact, a solid in solution exists in a chemical state known as solubility equilibrium. Each solubility equilibrium is defined by a temperature-dependent equilibrium constant (K_s). In a dynamic equilibrium as such, certain individual molecules migrate between the solid and solution phases at equal rates of dissolution and precipitation. When equilibrium is reached and the solid has not been completely dissolved, the solution is considered saturated. The concentration of a solute in saturated solution is known as the solubility (s), which is temperature dependent. A solution containing a higher concentration of solute than the solubility is said to be supersaturated, and it is under these conditions that a precipitate can form [45]. This occurs when the so-called solubility quotient (Q_s) (that has the same expression as K_s but with the concentrations at a specific point in time) is higher than the solubility constant K_s [46].

When the precipitate is a hydroxide of a metal ion (which can later be transformed into an oxide either through thermal treatment or spontaneously if the hydroxide form is unstable), K_s is usually defined as follows [43]:

$$M(OH)_{n(s)} \rightleftarrows M^{n+}_{(aq)} + nOH^-_{(aq)} \tag{7}$$

Table 8 Initial concentration, final pH after plasma exposure, precipitate that is supposed to form, Ks and Qs of precursors that do not necessitate a change of OS to form a precipitate in the final pH range obtained after plasma-exposure

Metal	Precursor	Initial cc (mol/L)	Final pH	Precipitate that can be formed [38]	Ks [38]	Qs
Al	$AlCl_3$	0.02	3.2	$Al(OH)_3/Al_2O_3$	10^{-34}	10^{-35}
Fe	$Fe(NO_3)_3$	0.01	2.3	$Fe(OH)_3/Fe_2O_3$	Between 10^{-37} and 10^{-42}	10^{-38}
	$FeCl_3$	0.01	2.4	$Fe(OH)_3/Fe_2O_3$	Between 10^{-37} and 10^{-42}	10^{-37}
Ti	$Ti(SO_4)_2$	0.01	1.6	$Ti(OH)_4/TiO_2$	Between 10^{-40} and 10^{-43}	10^{-52}

$$K_s = \left[M^{n+}\right][OH^-]^n \tag{8}$$

To determine whether a hydroxide can form in our plasma-exposed solution, we need to have $Q_s > K_s$, which is thus function of the amount of metallic ion M^{n+} and OH^- present in the medium. By considering this, we can calculate the Q_s of the precursors mentioned above since we know the concentration of M^{n+} introduced into the solution (from the initial concentration of the precursor) and the concentration of OH^- determined from the final pH measurement (Eq. 9) (Table 8) [43]. By doing that, we observe that, for all of these precursors, $Q_s < K_s$, which is coherent with the fact that no precipitate was observed.

$$pOH = 14 - pH,\ and,\ pOH = -\log\left[OH^-\right] \tag{9}$$

The solubility constant explains why these precursors did not form a precipitate by exposure to the glidarc plasma. Indeed, the initial concentration of the precursor used, and therefore of the metallic ions, was not high enough to fulfil the condition $Q_s > K_s$ and initiate precipitation. To confirm this, we attempted to expose a precursor containing Fe^{3+} and Al^{3+} ions at a higher concentration (0.03 mol/L) to the plasma, ensuring $Q_s > Ks$. Under these conditions, a precipitate formed. However, it is worth noting that precursors that do not require a change in OS to form the corresponding hydroxide do not necessitate plasma to precipitate. On the contrary, since hydroxides are the primary species involved in the precipitation, exposing the precursor to plasma, which generates

Table 9 Initial concentration, final pH after plasma exposure, precipitate that is supposed to form, Ks and Qs of precursors reacting by glidarc plasma to form a precipitate

Metal	Precursor	Initial cc (mol/L)	Final pH	Precipitate	K_s [38, 47]	Qs
Fe	$FeSO_4$	0.01	3	$Fe(OH)_3/Fe_2O_3$	Between 10^{-37} and 10^{-42}	10^{-35}
	$(NH_4)_2Fe(SO_4)_2$		3			10^{-35}
Mn	$Mn(CH_3COO)_3$	0.01	4.8	MnO_2	Insoluble	
	$KMnO_4$		3.2			
	$NaMnO_4$		3.2			
Sn	$SnCl_2$	0.01	1.6	$Sn(OH)_4/SnO_2$	Between 10^{-58} and 10^{-64}	10^{-51}
	$SnSO_4$					10^{-50}
Ti	$TiCl_3$	0.01	3.7	TiO_2	Insoluble	

H^+ species, tends to prevent the precipitation. Indeed, when we compared the precipitate formed from the $Fe(NO_3)_3$ precursor with or without exposure to the plasma, we obtained the same solid, confirming the lack of interest of plasma for these types of precursors (Supplementary information SI.3) (NB: To see the formation of a precipitate from a precursor containing Fe^{3+} ion at higher concentration, heating the solution was necessary either after plasma exposure for the GP synthesis or during the stirring for the non-GP synthesis).

This reveals another important parameter to consider before exposing any type of precursor, namely that the initial precursor concentration is high enough to allow the formation of a precipitate provided that a redox reaction can occur. Indeed, if we calculate the Q_s for all precursors that react by plasma (if possible), we observe that in every case, $Q_s > K_s$ (Table 9), in line with the formation of precipitates following the redox reaction in all these cases.

In conclusion to this part, the solubility of the precipitate formed is not a determining factor in whether a precursor will react by GP. However, it is important to consider this aspect to be able to observe the precipitate resulting from the redox reaction of the precursors with the plasma species. Therefore, solubility should be considered, as is the case for any usual precipitation process, after confirming that a precursor is expected to react by GP, before exposing it to the GP reactor.

Interest of the Plasma for Precursors That Spontaneously Form a Precipitate in Water

It also worth noting that some precursors forming a precipitate after GP exposure, tend to also undergo oxidation or reduction spontaneously in water. As previously discussed in Sect. "pH of the medium"., species located outside the zone between the lines “a” and

Table 10 Redox reactions between HNO_2/NO_2^- species or H_2O/H^+ and precursors exposed to the glidarc plasma that give a precipitate

Precursor/precipitate	Reaction with HNO_2 or NO_2^-		Reaction with H_2O or H^+ If metal reduction: $O_2 + 4H^+ + 4e^- \rightleftharpoons 2H_2O$ $E° = 1.23V$ If metal oxidation: $2H^+ + 2e^- \rightleftharpoons H_2$ $E° = 0V$	
	Number of electrons	ΔE (V)	Number of electrons	ΔE(V)
$KMnO_4$: $MnO_4^- + 4H^+ + 3e^- \rightleftharpoons MnO_2 + 2H_2O$ $E = 1.692 - 0.0788pH + 0.0197log\left(C_{MnO_4^-}\right) = 1.41V$	3	0.51; 0.32	12	0.18
$SnSO_4$; $SnCl_2$: $SnO_2 + 4H^+ + 2e^- \rightleftharpoons Sn^{2+} + H_2O$ $E = -0.077 - 0.1182pH - 0.0295log\left(C_{Sn^{2+}}\right) = -0.26V$	2	1.46; 1.26	2	0.26
$TiCl_3$ [38]: $TiO_2 + 4H^+ + e^- \rightleftharpoons Ti^{3+} + 2H_2O$ $E = -0.666 - 0.2364pH - 0.0591log\left(C_{Ti^{3+}}\right) = -1.11V$	1	2.31; 2.11	2	1.11

"b" on the Pourbaix diagram are not stable in water and tend to spontaneously transform into more stable ones found within this zone [38]. However, MnO_4^-, Sn^{2+} and Ti^{3+} precursors are all present outside this area, indicating that they tend to spontaneously transform into the solids also formed by GP. By employing a similar process to that used with HNO_2 and/or NO_2^- species, but this time using H_2O as a reactant (O_2/H_2O or O_2/O^{2-} if reduction, H_2O/H_2 or H^+/H_2 if oxidation), we observe that the ΔE values of the redox reactions of these three precursors with water indicate spontaneous reaction (Table 10) [38, 43]. However, we know that plasma makes the formation of these precipitates quicker. For example, while it takes days for $KMnO_4$ to precipitate into MnO_2 in water, with GP, a precipitate appears after only 4 min of exposure [29, 48].

In this context, the question arises as to whether we can anticipate the benefit of exposing a precursor to the GP rather than allowing it to react in water. To answer this, we need to consider the kinetics of the redox reactions. In fact, a redox reaction is more likely to occur if the number of electrons needed is smaller [42]. Furthermore, the greater the ΔE between 2 reacting couples, the quicker the reaction may occur [43]. In fact, for all the precursors that react by GP, we observe that the number of electrons needed is sometimes smaller and ΔE is always greater when reacting with plasma species (Table 10). This theoretically demonstrates the benefit of using plasma over allowing the reaction to occur in water, as calculations indicate that the redox reaction with GP-generated species are quicker than those with water species.

Application of the Identified Factors to Predict Precursors That May React By GP:

With the parameters we have identified, it is now possible to anticipate which precursors will react by GP to give a precipitate and which will not. To facilitate this approach, we have created a dichotomous key. This key allows to determine, step by step, whether a precursor may or may not fit the identified parameters identified crucial for its ability to react

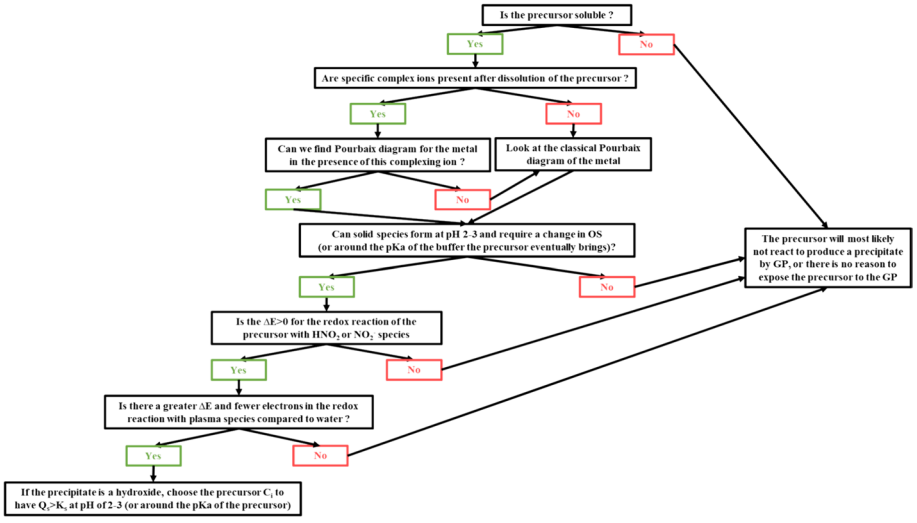

Fig. 4 Dichotomous key to determine whether a precursor may or may not to react and form a precipitate by GP

and form a precipitate by GP (Fig. 4). If we examine this dichotomous key in detail and explain how it works, we can see that the first step is to choose a precursor that is soluble in water as, currently, only aqueous solutions of a precursors are used and studied when exposed to the GP. Next, we need to identify which species are present upon the dissolution of the precursor, as mentioned in Sect. "Nature of the precursor:" “Nature of the precursor”. If a Pourbaix diagram of the formed metal ions is available, this tool allows us to quickly anticipate whether a precipitate can form at the type of pH we will have upon exposure, typically around 2–3 if the precursor does not act as a buffer, or around the pKa of the precursor. In fact, if no precipitate can be formed at such pH, there is no interest in exposing this precursor to the GP. If a precipitate can form, we still need to determine whether the metal ions present in solution would react with the plasma species by calculating the ΔE of the redox reaction between the precursor and the HNO_2/NO_2^- species, as mentioned in Sect. "Potential of the redox reaction" “Potential of the redox reaction”. For better prediction, it is preferable to calculate this ΔE using the actual E of the metal redox couple,

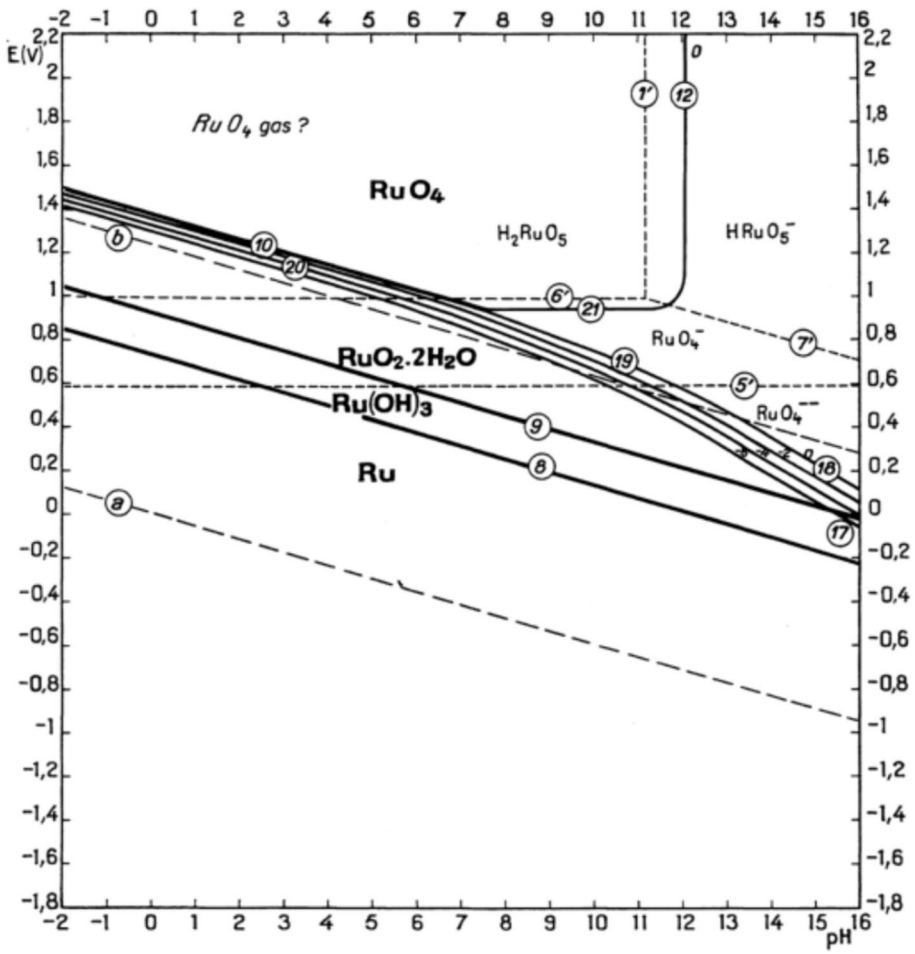

Fig. 5 Pourbaix diagram of Ru-water at 25 °C [38]

considering the concentration of the precursor we will use and the final pH we expect to have at the end of the exposure. If the ΔE indicates that no redox reaction with plasma species will occur, the precipitate is unlikely to form. On the other hand, if the ΔE suggests that the reaction will occur, it is still possible to assess the benefit of exposing the precursor to the GP rather than allowing it to react spontaneously in water. This assessment involves examining the number of electrons and the ΔE of the redox reaction between the precursor and water, as explain in Sect. "Interest of the plasma for precursors that spontaneously form a precipitate in water" "Interest of the plasma for precursors that spontaneously form a precipitate in water". Finally, before exposing the chosen precursor, we need to ensure that the initial concentration selected guarantees a Qs > Ks at the final pH we expect, as mentioned in Sect. "Solubility of the precipitate" "Solubility of the precipitate". This ensure that a precipitate will indeed form upon reaction, allowing us to recover it effectively.

By using this tool, two new precursors were identified as potentially reacting by GP: $HAuCl_4$ and $KRuO_4$.

For $KRuO_4$, the first parameter is respected as this precursor is soluble. In solution, it dissolves to release RuO_4^- and K^+, is the later being a spectator ion. As seen in the Sect. "pH of the medium", RuO_2, $Ru(OH)_3$ and Ru can all be formed under acidic pH conditions (Fig. 5) [38]. However, referring to the position of these solids with respect to RuO_4^- in the Pourbaix diagram, we observe that the formation of RuO_2 must precede the formation of $Ru(OH)_3$ or Ru species. Therefore, it is only interesting to determine if RuO_2 can be formed as, if not, other ruthenium-based solids will also not be able to form. To ascertain this, we calculated the ΔE for the redox reaction of RuO_4^- with HNO_2 or NO_2^- species to form RuO_2, which indicates that the reaction is feasible (Table 11). We can also confirm the interest of exposing this precursor to the GP rather than allowing it to simply react with water. By calculating the ΔE and the number of electrons involved in the redox reaction, it is evident that both values are respectively higher and smaller, when reacting with GP than with water species (Table 11). Finally, before exposing this precursor to the GP, we need to ensure that the initial concentration of $KRuO_4$ is high enough to have $Q_s > K_s$. However, as RuO_2 is considered completely insoluble, the initial concentration does not really matter [49]. To validate the theory that tells us that this reaction will work, we exposed a solution of 0.001 mol/L of $KRuO_4$ to the GP for 30 min and observed indeed the formation of a black precipitate after 1 min, corresponding to RuO_2 (supplementary information SI.4).

Table 11 Redox reactions between HNO_2 or NO_2^- or species and $KRuO_4$ precursor

$KRuO_4$ [38]:		
$RuO_4^- + 4H^+ + 3e^- \rightleftharpoons RuO_2 + 2H_2O$		
$E_0 = 1.533 - 0.0788pH + 0.0197log\left(C_{RuO_4^-}\right) = 1.238V$ (if pH = 3 and C_i $KRuO_4^-$ = 0.001 mol/L)		
NO_2/NO_2^- (Eq. 5) $E° = 0.9$ V	$RuO_4^- + 4H^+ + 3NO_2^- \rightleftharpoons RuO_2 + 3NO° + 2H_2O$	$\Delta E = 0.338V;3e^-$
NO_2/HNO_2 (Eq. 6) $E° = 1.09$ V	$RuO_4^- + H^+ + 3HNO_2 \rightleftharpoons RuO_2 + 3NO_2 + 2H_2O$	$\Delta E = 0.148V;3e^-$
$O_2 + 4H^+ + 4e^- \rightleftharpoons 2H_2O$ $E_0 = 1.23$ V	$4RuO_4^- + 4H^+ \rightleftharpoons 4RuO_2 + 3O_2 + 2H_2O$	$\Delta E = 0.008V;12e^-$

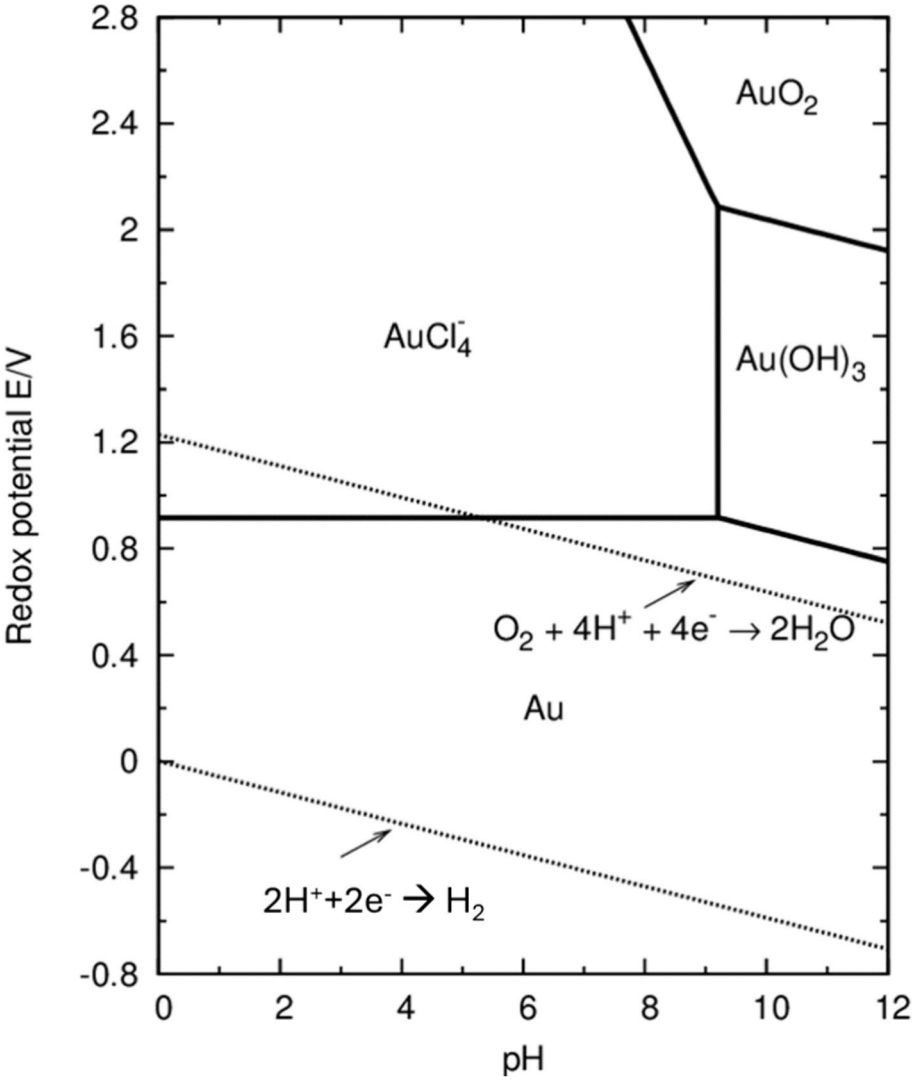

Fig. 6 Pourbaix diagram of Au-water-Cl^- at 25 °C [50]

In the case of $HAuCl_4$, the system is more complicated. This precursor is soluble and can potentially form the Au precipitate under acidic pH conditions (Fig. 6) [38]. However, when $HAuCl_4$ dissolves in water, it behaves as a strong Brönsted acid and dissociates into H^+ and $AuCl_4^-$ ions (Fig. 6) [50]. Furthermore, in aqueous solution, $AuCl_4^-$ undergoes spontaneous hydrolysis with different levels of hydroxylation depending on the pH (Eq. 10) [51, 52]. According to the literature, at pH around 2–3, the predominant species present in solution are $AuCl_4^-$, $[AuCl_3(OH)]^-$, and $[AuCl_2(OH)_2]^-$ [52, 53].

$$AuCl_4^- + jH_2O \rightleftharpoons AuCl_{4-j}(OH)_j^- + jCl^- + jH^+ \tag{10}$$

Table 12 Redox reactions between HNO_2 or NO_2^- species and $HAuCl_4$ precursor

$HAuCl_4$: $AuCl_4^-$: $AuCl_4^- + 3e^- \rightleftharpoons Au + 4Cl^-$ $E° = 0.97V$		
NO_2/NO_2^- (Eq. 5) $E° = 0.9$ V	$AuCl_4^- + 3NO_2^- \rightleftharpoons Au + 3NO_2 + 4Cl^-$	$\Delta E = 0.07V;3e^-$
NO_2/HNO_2 (Eq. 6) $E° = 1.09$ V	$AuCl_4^- + 3HNO_2 \rightleftharpoons Au + 3NO_2 + 3H^+ + 4Cl^-$	$\Delta E = -0.12V;3e^-$
$HAuCl_4$: $[AuCl_3(OH)]^-$: $[AuCl_3(OH)]^- + H^+ + 3e^- \rightleftharpoons Au + 3Cl^- + H_2O$ $E° = 1.07V$		
NO_2/NO_2^- (Eq. 5) $E° = 0.9$ V	$[AuCl_3(OH)]^- + H^+ + 3NO_2^- \rightleftharpoons Au + 3NO_2 + 3Cl^- + H_2O$	$\Delta E = 0.17V$ $;3e^-$
NO_2/HNO_2 (Eq. 6) $E° = 1.09$ V	$[AuCl_3(OH)]^- + H^+ + 3HNO_2 \rightleftharpoons Au + 3NO_2 + 3Cl^- + H_2O$	$\Delta E = -0.02V$ $;3e^-$
$HAuCl_4$: $[AuCl_2(OH)_2]^-$: $[AuCl_2(OH)_2]^- + 2H^+ + 3e^- \rightleftharpoons Au + 2Cl^- + 2H_2O$ $E° = 1.18V$		
NO_2/NO_2^- (Eq. 5) $E° = 0.9$ V	$[AuCl_2(OH)_2]^- + 2H^+ + 3NO_2^- \rightleftharpoons Au + 3NO_2 + 2Cl^- + 2H_2O$	$\Delta E = 0.28V$ $;3e^-$
NO_2/HNO_2 (Eq. 6) $E° = 1.09$ V	$[AuCl_2(OH)_2]^- + 2H^+ + 3HNO_2 \rightleftharpoons Au + 3NO_2 + 2Cl^- + 2H_2O$	$\Delta E = 0.09V$ $;3e^-$

Therefore, to determine if $HAuCl_4$ is able to react with HNO_2 or NO_2^- species to form Au^0, we first need to calculate the $E_{\left(\frac{[ML_y]^{z+}}{M}\right)}$ of these complexes using their formation constant K_f and the $E_{\left(\frac{M^{z+}}{M}\right)}$ of the redox couple $Au^{3+/}Au$ (Eq. 11–14, Table 12) [38, 54]. By calculating the ΔE of the redox reaction of these complexes with HNO_2 or NO_2^- species, we observe that all of them could achieve a redox reaction with at least NO_2^-.

Before testing this precursor, we selected a concentration in $HAuCl_4$ of 0.001 mol/L, as Au is considered as completely insoluble. Finally, when $HAuCl_4$ is exposed to the GP, we do obtain a precipitate, which is pure metallic Au (supplementary information SI.5).

$$Au^{3+} + 3e^- \rightleftharpoons AuE_1^\circ = 1.5 + 0.0197 \log\left(C_{Au^{3+}}\right) = 1.44V\left(ifC_{Au^{3+}} = 0.001mol/L\right) \tag{11}$$

$$Au^{3+} + 4Cl^- \rightleftharpoons \left[AuCl_4\right]^- K_f = 1 * 10^{24} \tag{12}$$

$$Au^{3+} + 3Cl^- + OH^- \rightleftharpoons \left[AuCl_3(OH)\right]^- K_f = 1 * 10^{19} \tag{13}$$

$$Au^{3+} + 2Cl^- + 2OH^- \rightleftharpoons \left[AuCl_2(OH)_2\right]^- K_f = 1 * 10^{13} \tag{14}$$

The formation of these two new precipitates suggests that the dichotomous key created to predict the formation of a solid upon exposure of a metal precursor to the GP is effective.

Conclusion

The objective of this paper was to investigate the parameters influencing the ability of specific precursors to react via humid air GP, leading to the formation of a precipitate. The aim is to enhance understanding of the method, ultimately enabling the synthesis of a wider range of catalysts and increasing the interest of GP as an innovative method for catalyst synthesis.

To achieve this objective, we adopted a strategy to identify commonalities between precursors that do form a precipitate via GP and those that do not react. The purpose was to determine the factors influencing the ability of a precursor to react. Since our method shares commonalities with the precipitation process, we sought to draw inspiration form this technique.

Several factors were identified as predominant in the ability of a precursor to react, including medium pH, standard potential of redox reactions, nature of the metal precursor and precursor and precipitate's solubility. Precisely, now we know that for a precursor to react by GP and form a precipitate, it is needed to:

1. Ensure that the precursor is soluble in aqueous medium.
2. Identify the actual species resulting from the dissociation of the precursors.
3. Identify if the metal can form a solid at acidic pH around 3 and that this formation necessitates a change of oxidation state of the metal.
4. Calculate whether the ΔE of the redox reaction between the precursor and HNO_2 and/or NO_2^- plasma species to form the solid are > 0.

5. Choose an initial concentration of precursor high enough to ensure that $Q_s > K_s$ for the precipitate.
6. Additionally, we can predict the potential interest of GP exposure over a simple water reaction by calculating the ΔE and the number of electrons needed for the precursor to undergo a redox reaction with water species. If the ΔE and number of electrons required are respectively higher and smaller with plasma species compared to water species, this indicates that GP exposure is advantageous.

These identified factors have enabled us to create a dichotomous key that can be used for any type of precursors that could be intended to expose to the GP, allowing to anticipate its potential reaction and precipitation. By utilizing this key, we have identified 2 new precursors that react by GP, forming new types of solids never before synthesized by this method: Au and Ru-based solids. This demonstrates that GP may be a promising method for developing new types of catalysts, such as metal-supported catalysts. However, it is important to note that this dichotomous key also indicates that only a limited number of precursors may react by plasma, at least without changing the conventional synthesis parameters we are currently employed. Therefore, this article not only highlights the new possibilities that the GP catalysts synthesis may offer, but also underlines its limitations.

Supplementary Information The online version contains supplementary material available at https://doi.org/10.1007/s11090-024-10516-1.

Acknowledgements Fanny Hanon acknowledges the FNRS for the FRIA scholarship no.40004581 and gratefully acknowledge François Devred for the technical and logistical support.

Author Contributions F.H. wrote the main manuscript text and E.G and M.D. helped in the interpretation of the results, structure of the text and corrections of the text.

Funding No funding other than the FRIA grant was provided for this manuscript.

Data Availability No datasets were generated or analysed during the current study.

Declarations

Conflict of interests The authors declare no competing interests.

References

1. Fadhel AZ, Pollet P, Liotta CL, Eckert CA (2010) Combining the benefits of homogeneous and heterogeneous catalysis with tunable solvents and nearcritical water. Molecules 15:8400–8424. https://doi.org/10.3390/molecules15118400
2. Ertl G, Knözinger H, Weitkamp J (1999) Preparation of solid catalysts. Wiley-VCH, New-York
3. Wang Z, Zhang Y, Neyts EC, Cao X, Zhang X, Jang BW-L, Liu C (2018) Catalyst preparation with plasmas: how does it work? ACS Catal 8:2093–2110. https://doi.org/10.1021/acscatal.7b03723
4. Kamgang-Youbi G, Herry J-M, Bellon-Fontaine M-N, Brisset J-L, Doubla A, Naïtali M (2007) Evidence of temporal postdischarge decontamination of bacteria by gliding electric discharges: application to hafnia alvei. Appl Environ Microbiol 73:4791–4796. https://doi.org/10.1128/AEM.00120-07
5. Czernichowski A (1994) Gliding arc: applications to engineering and environment control. Pure Appl Chem 66:1301–1310. https://doi.org/10.1351/pac199466061301
6. Lesueur H, Czernichowsky A, Chapelle J, Dispositif de génération de plasma basse température par formation de décharges électriques glissantes, 2639172

7. Ghezzar MR, Abdelmalek F, Belhadj M, Benderdouche N, Addou A (2007) Gliding arc plasma assisted photocatalytic degradation of anthraquinonic acid green 25 in solution with TiO_2. Appl Catal B 72:304–313. https://doi.org/10.1016/j.apcatb.2006.11.008
8. Tsagou-Sobze EB, Moussa D, Doubla A, Hnatiuc E, Brisset J-L (2008) Gliding discharge-induced oxidation of a toxic alkaloid. J Hazard Mater 152:446–449. https://doi.org/10.1016/j.jhazmat.2007.12.066
9. Czernichowski A, Nassar H, Ranaivosoloarimanana A, Fridman AA, Simek M, Musiol K, Pawelec E, Dittrichova L (1996) Spectral and electrical diagnostics of gliding arc. Acta Physica Polonica A 89:595–603
10. Doubla A, Boubabello L, Fotso M, Brisset J (2008) Plasmachemical decolourisation of bromothymol blue by gliding electric discharge at atmospheric pressure. Dyes Pigm 77:118–124. https://doi.org/10.1016/j.dyepig.2007.03.016
11. El-Zein A, Talaat M, El-Aragi G, El-Amawy A (2016) Electrical characteristics of nonthermal gliding arc discharge reactor in argon and nitrogen gases. IEEE Trans Plasma Sci 44:1155–1159. https://doi.org/10.1109/tps.2016.2578301
12. Brisset J-L, Moussa D, Doubla A, Hnatiuc E, Hnatiuc B, Kamgang Youbi G, Herry J-M, Naïtali M, Bellon-Fontaine MN (2008) Chemical reactivity of discharges and temporal post-discharges in plasma treatment of aqueous media: examples of gliding discharge treated solutions. Ind Eng Chem Res 47:5761–5781. https://doi.org/10.1021/ie701759y
13. Tiya-Djowe A, Laminsi S, Noupeyi GL, Gaigneaux EM (2015) Non-thermal plasma synthesis of sea-urchin like α-FeOOH for the catalytic oxidation of Orange II in aqueous solution. Appl Catal B 176–177:99–106. https://doi.org/10.1016/j.apcatb.2015.03.053
14. Tiya-Djowe A, Acayanka E, Mbouopda AP, Boyom-Tatchemo W, Laminsi S, Gaigneaux EM (2019) Producing oxide catalysts by exploiting the chemistry of gliding arc atmospheric plasma in humid air. Catal Today 334:104–112. https://doi.org/10.1016/j.cattod.2019.01.008
15. Brisset J-L, Pawlat J (2016) Chemical effects of air plasma species on aqueous solutes in direct and delayed exposure modes: discharge, post-discharge and plasma activated water. Plasma Chem Plasma Process 36:355–381. https://doi.org/10.1007/s11090-015-9653-6
16. Benstaali B, Boubert P, Cheron BG, Addou A, Brisset JL (2002) Density and rotational temperature measurements of the OH° and NO° radicals produced by a gliding arc in humid air. Plasma Chem Plasma Process 22:553–571. https://doi.org/10.1023/A:1021371529955
17. Moussa D, Vitrac H, Chéron BG, Hnatiuc E, Addou A, Brisset JL (2005) Acidity control of the oxidation reactions induced by non-thermal plasma treatment of aqueous effluents in pollutant abatment processes. Eur Phys J Appl Phys 29:308–312
18. Van Boxem W, Van der Paal J, Gorbanev Y, Vanuytsel S, Smits E, Dewilde S, Bogaerts A (2017) Anti-cancer capacity of plasma-treated PBS: effect of chemical composition on cancer cell cytotoxicity. Sci Rep 7:16478. https://doi.org/10.1038/s41598-017-16758-8
19. Khlyustova A, Labay C, Machala Z, Ginebra M-P, Canal C (2019) Important parameters in plasma jets for the production of RONS in liquids for plasma medicine: a brief review. Front Chem Sci Eng 13:238–252. https://doi.org/10.1007/s11705-019-1801-8
20. Burlica R, Kirkpatrick MJ, Locke BR (2006) Formation of reactive species in gliding arc discharges with liquid water. J Electrostat 64:35–43. https://doi.org/10.1016/j.elstat.2004.12.007
21. Gorbanev Y, Privat-Maldonado A, Bogaerts A (2018) Analysis of short-lived reactive species in plasma–air–water systems: the dos and the do nots. Anal Chem 90:13151–13158. https://doi.org/10.1021/acs.analchem.8b03336
22. Boyom-Tatchemo FW, Devred F, Ndiffo-Yemeli G, Laminsi S, Gaigneaux EM (2020) Plasma-induced redox reactions synthesis of nanosized α-, γ- and δ-MnO2 catalysts for dye degradation. Appl Catal B 260:118159. https://doi.org/10.1016/j.apcatb.2019.118159
23. Bruggeman PJ, Kushner MJ, Locke BR, Gardeniers JGE, Graham WG, Graves DB, Hofman-Caris RCHM, Maric D, Reid JP, Ceriani E, Fernandez Rivas D, Foster JE, Garrick SC, Gorbanev Y, Hamaguchi S, Iza F, Jablonowski H, Klimova E, Kolb J, Krcma F, Lukes P, Machala Z, Marinov I, Mariotti D, Mededovic Thagard S, Minakata D, Neyts EC, Pawlat J, Petrovic ZL, Pflieger R, Reuter S, Schram DC, Schröter S, Shiraiwa M, Tarabová B, Tsai PA, Verlet JRR, Von Woedtke T, Wilson KR, Yasui K, Zvereva G (2016) Plasma–liquid interactions: a review and roadmap. Plasma Sour Sci Technol 25:053002. https://doi.org/10.1088/0963-0252/25/5/053002
24. Zhu J, Gao J, Ehn A, Aldén M, Larsson A, Kusano Y, Li Z (2017) Spatiotemporally resolved characteristics of a gliding arc discharge in a turbulent air flow at atmospheric pressure. Phys Plasmas. https://doi.org/10.1063/1.4974266
25. Sun SR, Kolev S, Wang HX, Bogaerts A (2016) Coupled gas flow-plasma model for a gliding arc: investigations of the back-breakdown phenomenon and its effect on the gliding arc characteristics. Plasma Sour Sci Technol. https://doi.org/10.1088/0963-0252/26/1/015003

26. Acayanka E, Kuete DS, Kamgang GY, Nzali S, Laminsi S, Ndifon PT (2016) Synthesis, characterization and photocatalytic application of TiO2/SnO2 nanocomposite obtained under non-thermal plasma condition at atmospheric pressure. Plasma Chem Plasma Proc 36:799–811. https://doi.org/10.1007/s11090-016-9699-0
27. Mbouopda AP, Acayanka E, Boyom-Tatchemo FW, Kamgang GY, Nzeufa AM, Laminsi S, Richard D (2018) New-route synthesis of N-doped TiO_2 via exposing the $TiCl_3$ precursor to non-thermal quenched plasma at various times. Mater Chem Phys 206:224–231. https://doi.org/10.1016/j.matchemphys.2017.12.019
28. Tiya-Djowe A, Dourges M-A, Deleuze H (2020) Tuning the "O" vacancies density in SnO_2 nanocrystals during and after humid air plasma synthesis: implications on the photocatalytic performances under UV light. J Mater Sci 55:4792–4807. https://doi.org/10.1007/s10853-019-04335-5
29. Tatchemo FWB, Nzali S, Kamgang Youbi G, Tiya Djowe A, Saa DK, Acayanka E, Laminsi S, Gaigneaux EM (2017) Gliding arc plasma synthesis of MnO2 nanorods for the plasma-catalytic bleaching of azoïc amaranth red dye. Top Catal 60:962–972. https://doi.org/10.1007/s11244-017-0761-9
30. Boyom Tatchemo FW (2018) Synthèse par plasma d'arc glissant des dioxydes de manganèse MnO2 : application à la dégradation catalytique de la Tartrazine Jaune dans les eaux usées, Thèse, Université catholique de Louvain, Université de Yaoundé I
31. Tiya Djowe A (2014) Adsorbants et catalyseurs à base d'argile préparés par voie plasmachimique pour la dépollution des eaux résiduaires industrielles, Thèse, Université catholique de Louvain, Université de Yaoundé I
32. Seutcha R, Kamgang-Youbi G, Acayanka E, Vermile V, Devred F, Gaigneaux EM, Laminsi S (2023) Plasma-synthesis of various polymorphs of tungsten trioxide nanoparticles using gliding electric discharge in humid air: characterization and photocatalytic properties. Plasma Sci Technol 25:125502. https://doi.org/10.1088/2058-6272/ace235
33. Acayanka E, Tiya Djowe A, Laminsi S, Tchoumkwé CC, Nzali S, Poupi Mbouopda A, Ndifon PT, Gaigneaux EM (2013) Plasma-assisted synthesis of TiO2 nanorods by gliding arc discharge processing at atmospheric pressure for photocatalytic applications. Plasma Chem Plasma Proc 33:725–735. https://doi.org/10.1007/s11090-013-9455-7
34. Tiya-Djowe A, Ruth N, Kamgang-Youbi G, Acayanka E, Laminsi S, Gaigneaux EM (2018) FeOx-kaolinite catalysts prepared via a plasma-assisted hydrolytic precipitation approach for Fenton-like reaction. Microporous Mesoporous Mater 255:148–155. https://doi.org/10.1016/j.micromeso.2017.07.036
35. Hanon F, Hermans S, Gaigneaux EM (2024) What are the species involved in the gliding arc plasma synthesis of heterogeneous catalysts? Catal Today 430:114550. https://doi.org/10.1016/j.cattod.2024.114550
36. The International Centre for Diffraction Data, ICDD (2020) http://www.icdd.com/.
37. Ripin DH, Evans DA, pKa Table, (n.d.). chrome-extension://efaidnbmnnnibpcajpcglclefindmkaj/http://ccc.chem.pitt.edu/wipf/MechOMs/evans_pKa_table.pdf.
38. M. Pourbaix, (1967) Atlas of electrochemical equilibria in aqueous solutions, National association of corrosion engineers, Cebelcor, Texas, Bruxelles
39. Hanon F, Gaigneaux EM (2024) Post-discharge: an interesting step to improve heterogeneous catalysts synthesized by glidarc plasma? Chem Eng J 489:151088. https://doi.org/10.1016/j.cej.2024.151088
40. Hanon F, Gaigneaux EM (2024) Improving the synthesis of heterogeneous catalysts by gliding arc plasma using the "no-cooling system." Appl Mater Today 40:102408. https://doi.org/10.1016/j.apmt.2024.102408
41. Boyom-Tatchemo FW, Devred F, Laminsi S, Gaigneaux EM (2021) Temporal post-discharge reactions effect on the oxidative catalytic properties of plasma-synthesized α-MnO2 nanorods. Appl Catal A 616:118109. https://doi.org/10.1016/j.apcata.2021.118109
42. M. Szabó, G. Bellér, J. Kalmár, I. Fábián, (2017) The Kinetics and Mechanism of Complex Redox Reactions in Aqueous Solution: The Tools of the Trade, In: Advances in Inorganic Chemistry, Elsevier https://doi.org/10.1016/bs.adioch.2017.02.004.
43. Charlot G (1963) L'analyse qualitative et les réactions en solution, 5th edn. Masson & Cie, Paris
44. Granados-Fernández R, Montiel MA, Díaz-Abad S, Rodrigo MA, Lobato J (2021) Platinum recovery techniques for a circular economy. Catalysts 11:937. https://doi.org/10.3390/catal11080937
45. Mettler-Toledo International Inc all rights, Supersaturation and Crystallization, (n.d.). https://www.mt.com/ca/en/home/applications/L1_AutoChem_Applications/L2_Crystallization/Supersaturation_Application.html
46. Solubility Product Constant and Common Ion Effect - Free Sketchy MCAT Lesson, (n.d.). https://www.sketchy.com/mcat-lessons/solubility-product-constant-and-common-ion-effect

47. Feitknecht W, Schindler P (1963) Solubility constants of metal oxides, metal hydroxides and metal hydroxide salts in aqueous solution. Pure Appl Chem. https://doi.org/10.1351/pac196306020125
48. Rees T (1987) The stability of potassium permanganate solutions. J Chem Educ 64:1058. https://doi.org/10.1021/ed064p1058
49. American Elements, Ruthenium(IV) Oxide, American Elements (n.d.). https://www.americanelements.com/ruthenium-iv-oxide-12036-10-1
50. Korotcenkov G, Gulina LB, Cho B, Brinzari V, Tolstoy VP (2014) Synthesis by successive ionic layer deposition (SILD) methodology and characterization of gold nanoclusters on the surface of tin and indium oxide films. Pure Appl Chem 86:801–817. https://doi.org/10.1515/pac-2013-1102
51. Mironov IV, Makotchenko EV (2009) Equilibria in the system of aquachlorohydroxogold(III) complexes in aqueous solution. Russ J Inorg Chem 54:2010–2017. https://doi.org/10.1134/S0036023609120298
52. Deffernez A, Hermans S, Devillers M (2006) Preparation of carbon-supported Pd and Au-Pd catalysts via optimized adsorption of metallic complexes. Stud Surf Sci Catal 162:79–86. https://doi.org/10.1016/S0167-2991(06)80893-1
53. Đurović MD, Puchta R, Bugarčić ŽD, van Eldik R (2014) Studies on the reactions of $[AuCl_4]^-$ with different nucleophiles in aqueous solution. Dalton Trans 43:8620–8632. https://doi.org/10.1039/c4dt00247d
54. Mironov IV, Makotchenko EV (2009) The Hydrolysis of AuCl4− and the Stability of Aquachlorohydroxocomplexes of Gold(III) in Aqueous solution. J Solution Chem 38:725–737. https://doi.org/10.1007/s10953-009-9400-9